Thermogravimetric and Kinetic Analysis of Biomass and Polyurethane Foam Mixtures Co-Pyrolysis

H. Stančin[a,*], H.Mikulčić[a,c], N.Manić[b], D.Stojiljiković[b], M.Vujanović[a], X.Wang[c], N.Duić[a]

[a]University of Zagreb, Faculty of Mechanical Engineering and Naval Architecture, Ivana Lučića 5, 10000 Zagreb, Croatia
[b]University of Belgrade, Faculty of Mechanical Engineering, Kraljice Marije 16, Belgrade, Serbia
[c]Department of Thermal Engineering, Xi'an Jiaotong University, Xi'an, Shaanxi, Xianning West Road, Xi'an, China
[*]hrvoje.stancin@fsb.hr

Abstract

Alternative fuels are crucial for the decarbonisation of high-energy demanding processes. The utilisation of waste materials to produce alternative fuels is especially interesting since, the co-pyrolysis of waste plastics and biomass was lately introduced as promising method since the synergistic effect might enhance the product properties compared to those from individual pyrolysis. Furthermore, the utilisation of waste biomass, like sawdust, is interesting since it does not influence the sustainability of biomass consumption, and even more, it avoids the usage of raw feedstock. Thermogravimetric analysis is performed to determine the thermal degradation behaviour and kinetic parameters of investigated mixtures to find the most appropriate utilisation method. Co-pyrolysis was conducted for three mixtures with the following biomass/polyurethane ratios: 75-25 %, 50-50 %, 25-75 %, over a temperature range of 30-800 °C, at three heating rates 5, 10 and 20 °C/min, under an inert atmosphere. Obtained results were subjected to comprehensive kinetic analysis to determine effective activation energy using the isoconversional model-free methods and provide a detailed analysis of the samples' thermal degradation process. This work aimed to identify the main thermal decomposition stages during co-pyrolysis of biomass and polyurethane mixtures and provide the mixture composition's influence on the considered thermochemical conversion process.

1. Introduction

Recycling waste and end-of-life plastic materials represent serious issues nowadays, with the potential to arise even more in the future due to increased consumption. About 27 million tons of plastic waste is generated in the EU in 2018. Of which 31.1 % is recycled, 41.6 % is used for energy recovery while the rest is landfilled, implying the irrevocable loss of valuable resources [1]. This problem is especially evident in complex plastics waste, which is not built by polymerisation but synthesised from different compounds, like polyurethane foam [2]. Polyurethane foams (PUF) are among the most used polymers worldwide, utilised in a flexible or rigid form for automotive purposes or as insulation and structural material. By selecting different polyols and isocyanates, the primary building block of PUF, the

manufacturer can produce more than 150 different foam types. Moreover, the PUF is often treated with various flame retardants due to application requirements, which complicates their recycling procedure [3]. Lately, thermochemical conversion into useful chemicals or fuels is proposed as a potential method to deal with its disposal problem. The pyrolysis is especially interesting since valuable liquids, gases, and biochar are obtained, which can be further utilised where appropriate [4]. Stančin et al. studied thermal degradation of waste rigid polyurethane foam (PUR) by thermogravimetric analysis (TGA), intending to investigate particle size's influence on solid residue chemical composition. They found a significant amount of harmful and hazardous compounds that constrain the direct application of obtained products. Major unwanted compounds found are various benzene-based species, chlorine-containing compounds, polycyclic aromatic hydrocarbons (PAHs), furans, and similar [5]. Guo et al. conducted catalytic gasification of PUR to maximise the hydrogen yield. Calcium carbonate had the best catalytic effect and promoted a significant amount of hydrogen (~80 vol.%), offering an alternative thermochemical route for PUR recycling [6]. Numerous researchers widely investigated the kinetics of polyurethane foams over the years by conducting TGA. The kinetic and thermodynamic analysis is useful for getting a good insight about the changes of a kinetic model during the process, but also to investigate the favorable process conditions to achieve predetermined goals of the considered thermochemical conversion process. Finally, kinetic and thermodynamic analysis results can serve as a basis for potential numerical modeling and simulations [7]. Garrido and Font [8] investigated a flexible PUF decomposition mechanism, at different heating rates, with the final temperature of 900 °C. They concluded that in the first degradation stage, urethane bonds are broken to produce isocyanates, while in the second stage, ether polyols are decomposed forming, mostly a solid residue. Yao et al. [9] recently performed a kinetic analysis of PUR from the discharged refrigerator, confirming the three-stage decomposition mechanism and the Flynn–Wall–Ozawa method as the most reliable for obtaining activation energies of PUF decomposition. Mikulčić et al. [10] investigated the thermal decomposition of PUR under different atmospheres. They concluded that the decomposition mechanism under the oxygen-enriched atmosphere could be roughly divided into two stages, starting with the devolatilisation and followed up by the oxidation of residues.

Various waste biomass was widely investigated as the prominent feedstock for sustainable alternative fuel production through pyrolysis or co-pyrolysis [11]. Nevertheless, due to complex biomass composition, their thermal degradation behaviour dramatically varies [12]. Luo et al. [13] conducted the pyrolysis on beech sawdust and used model-free analysis to assess activation energies. The thermal decomposition was divided into three stages by observing the extent of conversion. Additionally, activation energies are calculated with the conclusion that Friedman's method corresponds to the real values. Zhang et al. [14] investigated the thermal decomposition of wood sawdust. Once again, it was confirmed that the sawdust decomposition consists of three steps, being the most intensive in the second one, where mostly cellulose and hemicellulose are decomposed. In addition, it was concluded that sawdust pyrolytic kinetic consists of multi-step reactions due to the presence of pseudo components, which decomposes independently. Manić et al. [15] carried out multi-component modeling kinetics and thermal analysis of apricot kernel shell using four pseudo-components. The analysis showed that the cellulose component dominant the

process, and the influence is slightly increased when higher heating rates are applied. Most of the studies deals with co-pyrolysis of biomass or sawdust from one type of wood. Alam et al. [16] investigated the co-pyrolysis of bamboo sawdust and low-density polyethylene, concluding that the higher heating rates shift the peak temperature toward higher values and broaden the temperature range in which decomposition takes place. Other works deal with co-pyrolysis of torrefied poplar wood with polyethylene [17], oak wood with different types of waste plastics [18], eucalyptus biomass residue with polystyrene [19], pine woodchips with the six most common plastics waste [20]. As can be seen, most of the studies deal with the individual analysis of polyurethane kinetics. The extended results which would cover the thermodynamic perspective are widely missing. On the other hand, various biomass feedstock was widely investigated in numerous research. Nevertheless, the work where sawdust mixture composed of different types of biomass is co-pyrolyzed with PUR is not found in the literature. The introduction of polyurethane to the co-pyrolysis process extends the state-of-the-art of polyurethane decomposition analysis. The inclusion of the thermodynamic part complements the knowledge gap of thermal decomposition investigation by broadening the knowledge on the influence of mixture composition on process dynamics.

This work reveals the thermogravimetric analysis (TGA) and kinetic analysis of waste biomass sawdust (SD) composed from different types of wood and PUR. As already mentioned above, PUR recycling requires complicated procedures; therefore, thermochemical recycling routes might be a promising alternative. Thermogravimetric analysis is used in this study to obtain necessary kinetic parameters such as activation energy, pre-exponential factor, and similar. In addition, we have provided an analysis of thermodynamic parameters, which are seldom in the literature. Since the decomposition mechanism of PUR is more similar to biomass than plastics, it is of great interest to investigate their interaction during the process and mutual influence on kinetic and thermodynamic parameters. The results from this study can be used to evaluate the feedstock suitability for co-pyrolysis and even more to provide a comprehensive insight for determining optimal process conditions such as mixing ratio, heating rate, and final temperature. Therefore, the main novelty of this work lies in the fact that for the first time, sawdust and polyurethane were investigated in fuel blend with an aim to derive appropriate conclusions regarding the feedstock suitability for the process and backed up by analysis of favorable process conditions.

2. Materials and methods

2.1 Materials and experimental procedure

The samples used in this study were waste sawdust mixture composed of fir, oak, and beech wood obtained from a local sawmill, while the PUR was previously used as an insulation material for refrigerators. Investigations were carried out for individual and mixture samples with the following shares: 25% PUR, 50% PUR, and 75% PUR. The sample preparation was done according to the standard procedure [21]. In addition, the samples were tested to obtain data of ultimate and proximate analyses following the relevant standard [22]. Results are given in Table 1. Selected particle sizes of the samples were between 0.125-0.25 mm, to

ensure homogeneity of the mixture. In addition, in the previous research [5], it was determined that this is the optimal particle size of selected PUR regarding the yield of organic compounds, especially those that might represent a threat to human health such as PAHs, furans, benzene containing compounds, and similar. Sample masses were about 10 mg, which is widely used for TGA. Samples were heated from room temperature up to 800 °C, since higher temperatures are applied for gasification. Different heating rates were used to investigate the influence of this parameter on process kinetics. As an inert carrier gas, Argon was used to avoid reactions with released volatiles. Furthermore, the prepared sample was also conducted to the Simultaneous Thermal Analysis (STA), which provides data for TGA and DTA simultaneously on the same sample. The NETZSCH STA 445 F5 Jupiter system was used for STA measurements under the following conditions:

- particle size 0.125-0.25 mm
- sample mass: 10 ± 0.5 mg.
- temperature range: from room temperature to 800 °C.
- heating rates: β = 5, 10 and 20 °C/min.
- the carrier gas: pure Argon with the total gas flow rate of 70 mL/min.

Table 1 - Results of Ultimate and Proximate analysis of investigated samples

Sample	Ultimate Analysis[a] (wt.%)					Proximate analysis (wt.%)				HHV (MJ/kg)
	C	H	O[b]	N	S	Moisture	Volatiles	Fixed carbon	Ash	
PUR	63.90	6.45	16.96	6.74	-	2.71	82.01	9.51	5.78	26.73
SD	47.33	6.04	44.77	0.31	0.02	7.35	72.95	18.28	1.42	17.30

[a]On a dry basis
[b]By the difference

2.2 Methods for calculation of energy activation and thermodynamic parameters

In this work, model-free methods were used to avoid potential errors in the calculation of energy activation that might arise from the misidentification of an appropriate kinetic model. Since the biomass decomposition is extremely complex, and the sawdust mixture is composed of different types of biomass, the probability of selecting the wrong model was too high. In addition, model-free analysis opens an opportunity to investigate the change of activation energy in dependence with the extent of conversion, suggesting the changes in reaction mechanisms and kinetics. If model-fitting methods are applied, one can only extract the average value for the whole process, which is not beneficial for the analysis of the reaction model and kinetics of the process.

Activation energies are calculated using the four model-free isoconversional methods, Friedman (Eq. 1), Kissinger-Akahira-Sonuse (KAS) (Eq. 2), Ozawa-Flynn-Wall (OFW) (Eq. 3), and Starink (Eq. 4):

$$\ln(\beta \frac{d\alpha}{dT}) = \ln[Af(\alpha)] - \frac{E}{RT} \qquad \text{Eq. 1}$$

$$\ln(\frac{\beta}{T^2}) = \ln\left[\frac{AR}{EG(\alpha)}\right] - \frac{E}{RT} \qquad \text{Eq. 2}$$

$$\ln\beta = \left[\frac{0.0048 * AE}{RG(\alpha)}\right] - 1.052(\frac{E}{RT}) \qquad \text{Eq. 3}$$

$$\ln(\frac{\beta}{T^{1.92}}) = C_s - 1.0008\frac{E}{RT} \qquad \text{Eq. 4}$$

In the equations mentioned above, α represents the degree of conversion, β is the heating rate, T is the temperature A, E, and R are the pre-exponential coefficient, the activation energy, and the universal gas constant, respectively. Activation energies in the Eq.1-4 are calculated as a function of the extent of conversion (α). In Eq. 1, Friedman's method for a different α value, a set of $\ln(\beta(d\alpha/dT))$ and $1/T$ pairs corresponding to each heating rate were collected and plotted to a straight line. The slope of each straight line, $(-E/R)$, was used to obtain the activation energy. In Eq. 2, for the KAS method, at each degree of conversion, the pairs of $\ln(\beta/T^2)$ and $1/T$ data points were obtained and plotted once again to a straight line. The slope $(-E/R)$ is then used to calculate the activation energy. In the case of the OFW method (Eq. 3), data points are collected for pairs of $\ln\beta$ and $1/T$ which were fitted to a straight line. From the slope $(-1.052(E/R))$, activation energy is calculated. In the Starink method (Eq. 4) at a given extent of conversion α, the data points of $\ln(\beta/T^{1.92})$ versus $1/T$ are plotted to a straight line at different temperature heating rates, and the slope of the line corresponds to $-1.0008E/R$. Therefore, the apparent activation energy E is calculated from the slope of the straight line.

Thermodynamic parameters, including the pre-exponential factor, are calculated using the following equations 5-8:

- Pre-exponential factor (A)
$$A = \frac{\beta * E * \exp(\frac{E}{R * T_m})}{R * T_m^2} \qquad \text{Eq. 5}$$

- Changes of enthalpy (ΔH)
$$\Delta H = E - RT_\alpha \qquad \text{Eq. 6}$$

- Changes in entropy (ΔS)
$$\Delta S = \frac{\Delta H - \Delta G}{T_m} \qquad \text{Eq. 7}$$

- Changes of free Gibbs energy (ΔG)
$$\Delta G = E + R * T_m * \ln(\frac{K_B * T_m}{h * A}) \qquad \text{Eq. 8}$$

Where K_B represents Boltzmann constant (1.381×10^{23} J/K), h Plank constant (6.626×10^{34} Js), T_m the DTG peak temperature, and T_α the temperature at the degree of conversion α [23]. To calculate the pre-exponential factor from Eq. 5, it was assumed the first-order kinetic

reaction with the kinetic model $f(\alpha) = (1-\alpha)$. As can be seen from equations 6-8, the pre-exponential factor A, and activation energy E are mandatory to calculate enthalpy changes, entropy, and free Gibbs energy.

2.3 Error analysis of experimental work

Regarding the error analysis of the experimental work, the proximate and ultimate analysis was performed according to standard test methods, which already include the defined procedures for measurement accuracy and measurement error handling. These procedures were applied to the data of proximate and ultimate analysis presented in this paper, and the obtained experimental values are presented according to the standard test requirements and common practice of presenting this type of data on a defined basis in order to be comparable with the literature data.

With regard to TG-DTG experimental work, the error analysis considers a comprehensive calibration and measurement procedure that precedes the sample measurement. The calibration procedure defined by the equipment manufacturer provides the accuracy of the measurement and is performed once every six months. The calibration procedure considers the used protective gas for the balance and selected heating rate. Furthermore, before each measurement to correction of the signals is performed by measurements with empty crucibles to correct the measured signals and handle the mass balance deviations. After that, the measurement with the crucible with the sample and reference crucible is performed and obtained correction signal is applied on measurement data through the manufacturer software used for the analysis. Those are common procedures for this type of experimental equipment which guarantee the accuracy of the measurements declared by the equipment manufacturer.

3. Results

3.1 Thermogravimetric analysis of sawdust and polyurethane foam samples

Figure 1 presents the thermogravimetric (TG) and derivative thermogravimetric curves (DTG) for individual sample pyrolysis, obtained at two different heating rates. The PUR decomposition can be roughly divided into three stages, already reported by Yao et al. [9]. Up to 200 °C, the sample's decomposition is barely visible, and the mass loss is below 3.5% for all investigated heating rates. The onset temperature for the second stage is at approximately 300 °C, and 303 °C for the heating rates of 5 and 10 °C/min, while the onset temperature for the heating rate of 20 °C/min is slightly higher ~311 °C. The decomposition peak is identified at 328 °C (5 °C/min), and it is further shifted to higher temperatures with the increment of heating rates to 338 and 348 °C, respectively. Similar values and trends for peak position are also reported by Xu et al. [24]. The first peak in DTG curves ends in the temperature range between 380 and 406 °C, and the endpoint is shifted toward a higher temperature with the heating rate increment. The remaining masses at this point are ~47% for 5 and 10 °C /min, while higher mass loss is noticed for the heating rate of 20 °C/min (42.5%), which is expected since the temperature range is shifted toward higher values for more than 20 °C. This first peak represents the main degradation stage, where mostly urethane bonds are broken, and isocyanates and polyols are decomposed [25,26]. The second flat peak immediately follows the end of the first peak. The second peak of the DTG curve

can be explained as a secondary cracking of 1,1-Dichloro-1-fluoroethane and similar halogenated compounds in an inert atmosphere and degradation of the soft segment [4]. Jiao et al. [27] studied the degradation characteristics of PUR under inert and oxidative atmosphere, and they found that this second peak is even more expressed in an oxidative environment. Besides, the increment of heating rate had a visible impact on this stage of degradation, being more pronounced for higher heating rates and broadening the temperature range in which decomposition happens. At approximately 480 °C, this second stage ends, and all samples have an almost identical mass loss, between 60 to 70% of the initial mass. Nevertheless, in the last stage, the mass loss is more intensive for higher heating rates, even though, in general, thermal decomposition in this stage is almost negligible. The final mass differs for investigated samples, being the lowest for 20 °C/min (19.7%), and highest for 5 °C/min (23.3%). By observing the TG and DTG curves, the increment of heating rate broadens the temperature range in which thermal degradation is happening and promotes the sample decomposition.

The sawdust decomposition also consists of three steps, starting with the moisture evaporation (~5% of mass loss), being followed by the most intensive second stage where mostly hemicellulose and cellulose content is decomposed (>60% of mass loss), and finally slow decomposition of the lignin content until the end of the process (~10 % of mass loss). For the heating rate of 5 °C/min, the first stage ends at 110 °C, after which the curve remains flat until 220 °C, where degradation slowly starts to progress once again. The first stage for higher rates goes up to ~140 °C, where most of the moisture is evaporated. The second stage begins at approximately 290 °C for 5 °C/min, and with the further increment of heating rate is shifted toward higher values to 296 and 302 °C, respectively. As can be seen, the increment of heating rate broadens the temperature range in which decomposition is happening, similar to PUR, and also shifted the peak in DTG curves from 342 to 352 and 358 °C, respectively. This phenomenon where the increment of heating rate shifts the temperature range toward higher values is already reported in several studies [28,29]. Mainly this is due to the heat transfer limitations and existence of temperature gradient between the surface and inner part of the particles, which influences the release of volatiles [16]. The main peak corresponds to the decomposition of the cellulose content [14]. The small shoulder in the peak can be noticed at 5 °C/min, corresponding to hemicellulose degradation. As the heating rate increase, this shoulder becomes less visible, already reported for sawdust decomposition [30]. The second stage ends at 370 °C for the 5 °C/min, and at 376 °C and 383 °C for the heating rates of 10 and 20 °C/min, respectively. At the end of this stage remaining mass is approximately 26% for all samples. In the last stage, mass loss follows the linear pathway until the end of the process, even though there is no visible mass loss after 600 °C. This last stage accounts for the degradation of the lignin content. The final mass is slightly lower for 5 °C/min (19.6%) compared to the other two samples, where the final mass is about 20.6%.
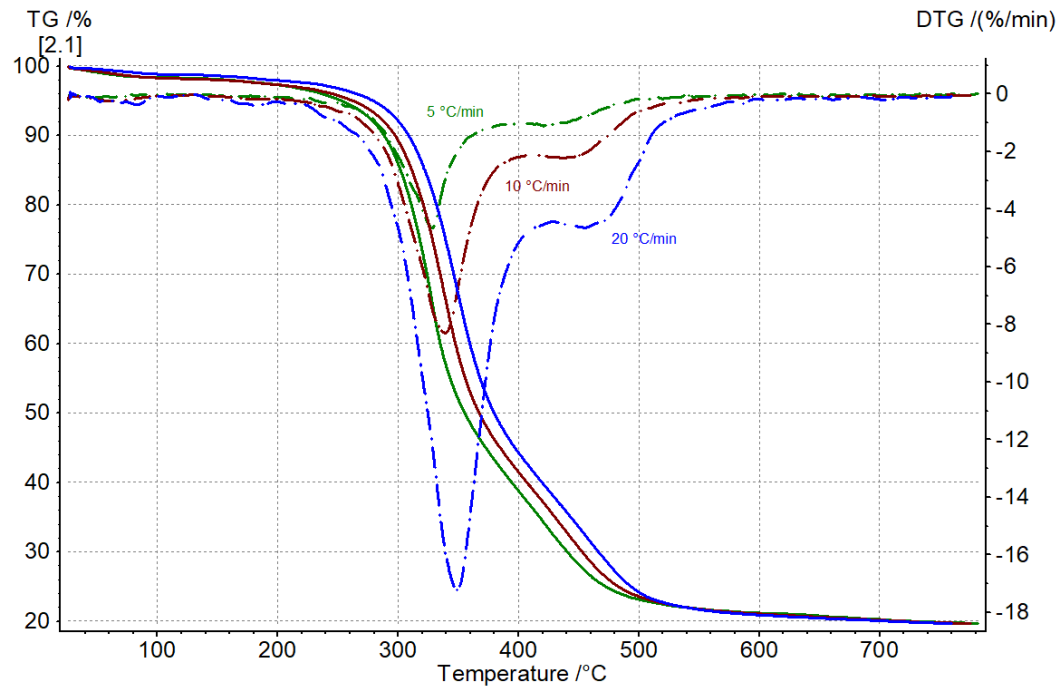
(a) PUR
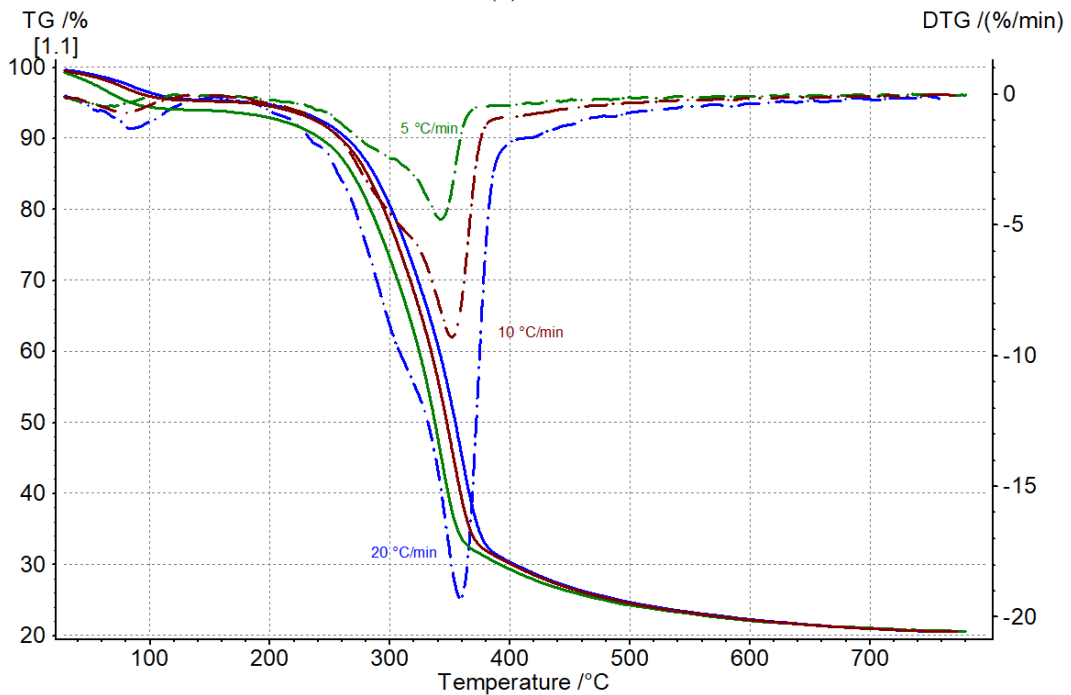
(b) Sawdust

Figure 1 – TG (solid lines) and DTG (dotted lines) curves from PUR (a) and Sawdust (b) pyrolysis

3.2 Thermogravimetric analysis of sawdust and polyurethane foam mixtures

Regarding the thermal decomposition of the investigated mixtures, it is observed from TG curves (Figure 2) that the sample where sawdust is a dominant compound express similar behaviour to the decomposition of the individual SD. In contrast, for the mixtures with 50 and 75% of PUR content, the decomposition is similar to the individual PUR sample. The first stage is slightly influenced by the introduction of PUR content to the mixture. As the

content of PUR increases, the mass loss decrease, as expected since this is mostly due to moisture evaporation. Regarding the heating rate, the first stage seems to be poorly influenced by this parameter, and mixture composition plays a more important role [29]. The only visible difference is at a heating rate of 5 °C/min, where slightly greater mass loss is noticed, similar to the SD sample.

The second stage onset temperature is poorly influenced by the mixture composition since the temperatures are in a similar range, while the more pronounced difference is for various heating rates. For the mixture with 25% of PUR, onset temperature increase with the increment of heating rate and are 280, 290, and 298 °C, respectively. The peak temperatures are also shifted toward higher values with the heating rate increment from 338 to 354 °C, noticed for other mixtures. The difference between peak temperature is negligible for the mixture with 50 and 75% of PUR content but still increase from 328 °C to 334 and 344 °C, as the heating rate increase. The end of the first peak is at 360 °C for 5 °C/min for all mixtures, which slightly increases with the increment of heating rate and PUR content in the mixture. For the heating rate of 20 °C/min, the end temperature of the first peak increase with the increment of PUR content to approximately 376, 380, and 400 °C, respectively. The first peak's end is immediately followed by the second one, similar to individual PUR pyrolysis. Precise determination of the second peak-end temperature is difficult, but it can be arbitrarily taken at about 500 °C since, at these points, DTG curves are very close to zero. Even though it should be emphasized that the second peak is more influence by the heating rate and mixture composition. With both parameters increment, the end temperature tends to shift toward values higher than 500 °C. In this second stage, the sample with 25% of PUR expresses similar behavior compared to the SD, while mixtures with 50 and 75% of PUR are closer to the individual PUR decomposition. The final temperature of the second stage is greatly influenced by both factors, mixture composition and heating rates. For the former one, it can be seen that the introduction of PUR broadened the temperature range in which decomposition takes place. Simultaneously, the second peak from the PUR degradation is smoothened and less pronounced in the DTG curve. This implies that biomass hinders secondary cracking of 1,1-Dichloro-1-fluoroethane, and with a higher share of biomass fraction in an investigated mixture, this peak is significantly reduced. For the mixture where SD is the dominant compound, the influence of both parameters is more visible compared to the rest of the samples.

The influence of the heating rate on the last stage of degradation is almost negligible. The mass of the residues at 600 °C is almost the same for all investigated heating rates and mixtures, except at 5 °C/min for the mixture with 25% of PUR, where the final mass is slightly lower. Lower final mass at a lower heating rate is expected since, in this case, sufficient time is provided for the complete release of volatiles. Besides, with the increment of PUR content in the mixture, the final mass of the residue is increased. Interestingly, with the increment of heating rate, the final mass decrease for the mixture with 50 and 75% of PUR, also noticed for the individual PUR decomposition. On the other hand, for the mixture with 25% of PUR, the final mass increase with the increment of heating rate, also observed for pure SD degradation.

In general, from the TG and DTG curves, it can be seen that the decomposition areas of individual samples overlap and taking place in a similar temperature range, which is very

beneficial for the occurrence of the synergistic effect between them. The existence of synergy can be confirmed by the final mass of investigated mixtures, which are higher than those from individual pyrolysis or theoretically expected. The existence of synergy can also be seen from the second peak of the second stage since the biomass influenced its intensity. The DTG curves are considerably smoothened compared to individual PUR pyrolysis, indicating that the sawdust has an important role in this temperature range for the decomposition intensity. Simultaneously, the PUR influence on the first stage of decomposition and the onset temperature for the second stage seems to be limited. In contrast, a more significant influence is noticed for the end temperature of this stage and the overall process. An increase of PUR content increased the final mass of the residue for all investigated mixtures. Regarding the heating rate, for the mixture with 25% of PUR, increment in the heating rate increased the final mass of the residue, observed for individual SD decomposition, while the opposite trend is noticed for the mixture with 50 and 75% of PUR content. Results are summarised in Table 2.
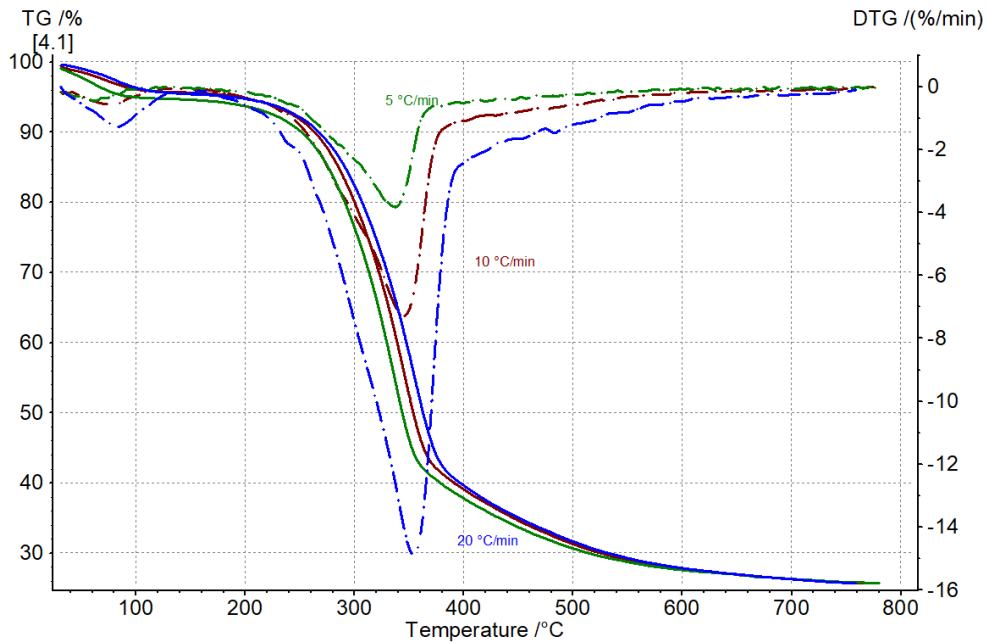
(a) 25% PUR
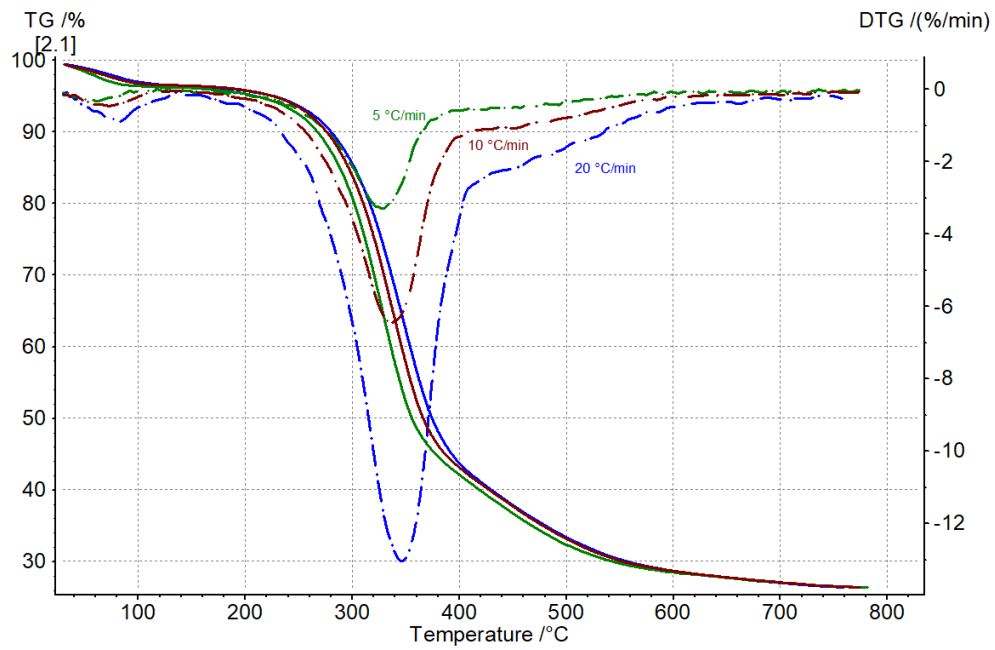
(b) 50% PUR
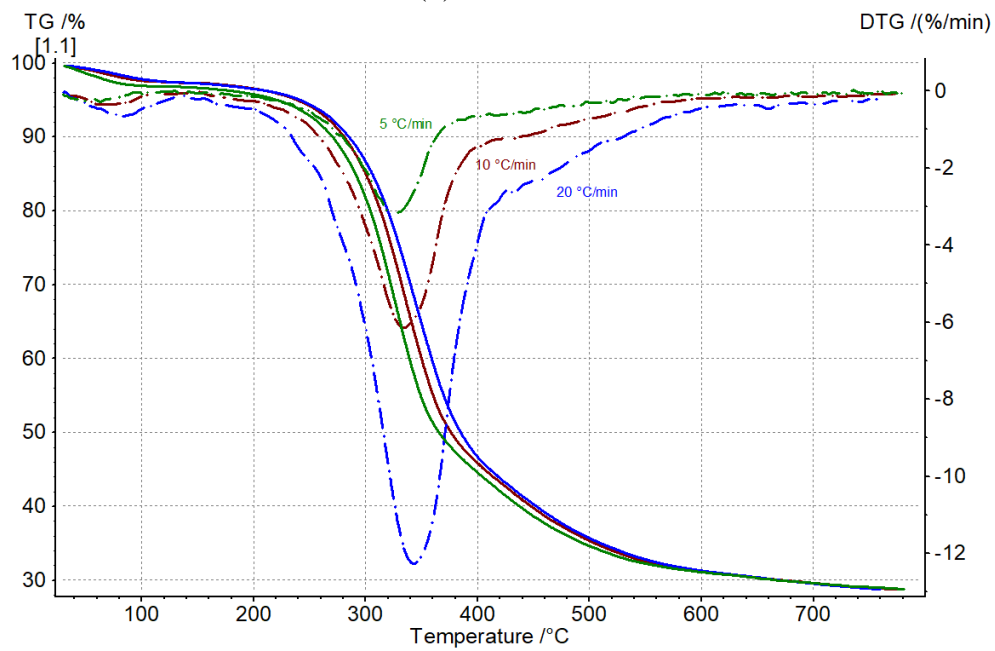
(c) 75% PUR

Figure 2 – TG (solid lines) and DTG (dotted lines) curves from sawdust and PUR mixture pyrolysis a) 25% PUR b) 50% PUR c) 75% PUR

Table 2 - Final masses from individual and mixture pyrolysis at various heating rates

Final mass [%]	5 °C/min	10 °C/min	20 °C/min
Sawdust	19.6	20.6	20.7
25% PUR	22.9	24.9	25.7
50% PUR	27.2	26.4	26.6
75% PUR	28.8	28.6	28.1
PUR	23.3	21.8	19.7

3.3 The activation energy of individual samples and their respective mixtures

The activation energy (E_a) was calculated using the model-free isoconversional Friedman, Kissinger-Akahira-Sonuse, Ozawa-Flynn-Wall, and Starink methods. Obtained values show excellent statistical correspondence by observing the statistical R^2 factor (>0.94947) for the range of conversion between α=0.1-0.9. Below and above these points, obtained activation energies show bigger discrepancies and lower statistical agreement, already reported in the literature [14]. In general (Figure 3a-e), it can be seen that there are only slight differences between the used methods. Moreover, the only visible differences are spotted between Friedmann and other methods, while the results from the KAS, OFW, and Starink greatly correlate.
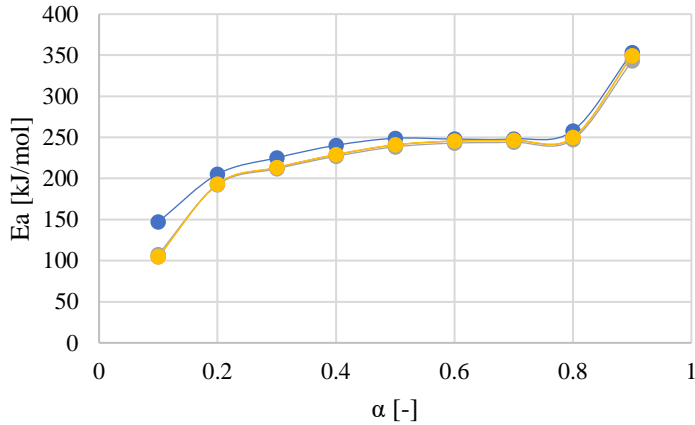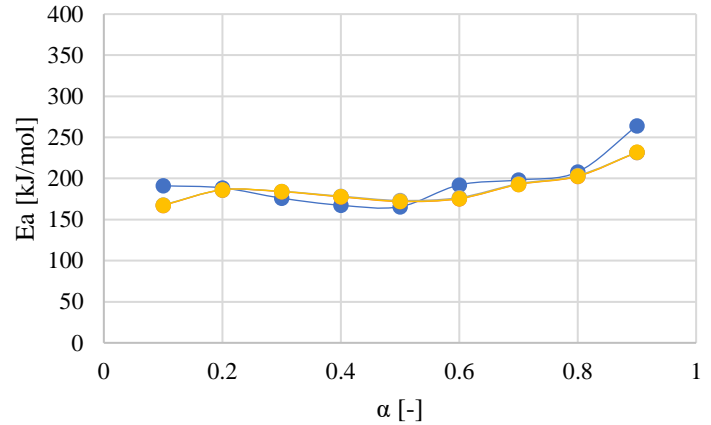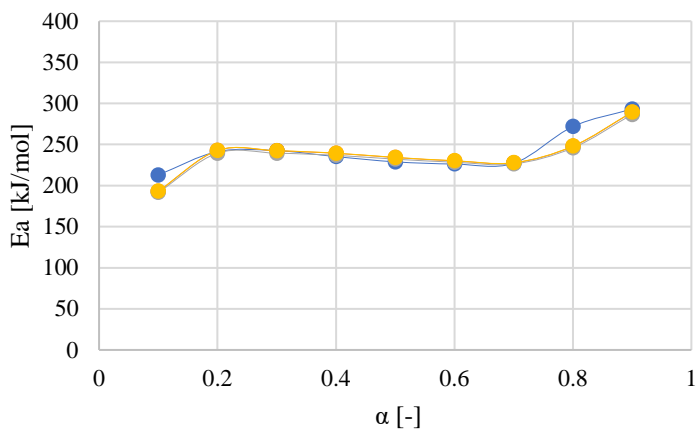
a) Sawdust

b) PUR

c) 25% PUR
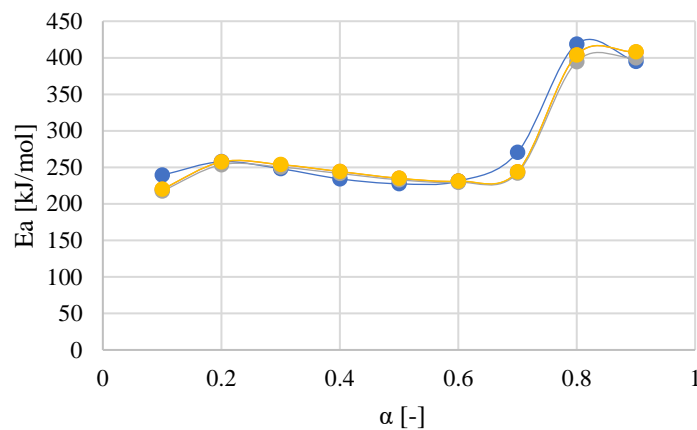
d) 50% PUR
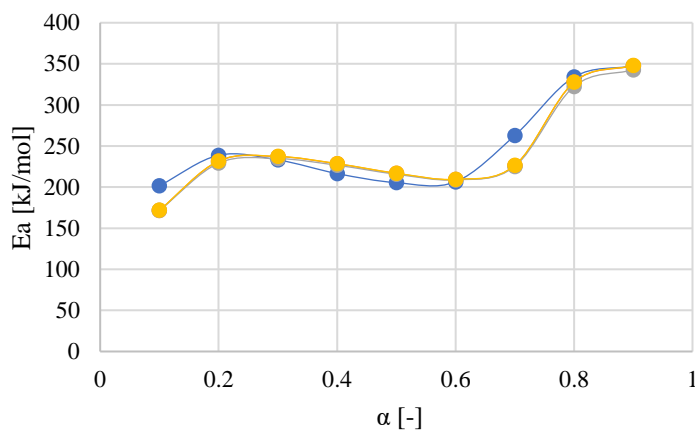
e) 75% PUR

Figure 3 - Calculated activation energies for individual samples and respective mixtures

The E_a of polyurethane is lower than the rest of the plastics, and it depends on the isocyanate index, which represents the hard segment of the PUFs. With the increment of this parameter, the E_a tends to increase, representing the existence of the stronger bonds in such a composition. Reported mean values in the literature differ but are in general below 200 kJ/mol [31], which is significantly lower compared to the polyethylene (PE), polystyrene (PS), or polypropylene (PP), where mean values are ~250 kJ/mol [32]. The mean activation energy of PUR used in this work is about 192 kJ/mol for KAS, OFW, and Starink method with an excellent statistical agreement (R^2>0.9970), while a slightly higher value (~202 kJ/mol) is obtained using the Friedman method, once again with a remarkable statistical agreement (R^2=0.9985).

Firstly, activation energy sharply increases up to α=0.1 (E_a~200 kJ/mol), suggesting that a higher amount of energy is required to initiate PUR decomposition. In the range of α=0.1-0.5, E_a gradually decreases to approximately 165 kJ/mol. In this stage, urethane bonds are broken, allowing the thermal decomposition of isocyanates and polyols. In the range

between α=0.5-0.6, it is noticed a bounce to 190 kJ/mol, which clearly shows the two-degradation mechanism that occurs during the PUR decomposition [26]. This is followed up by a constant increase until α=0.8. At this point, most of the sample is already decomposed, resulting in the steep increment of E_a. As can be seen, calculated values using different methods show great similarity. The difference between Starink and KAS methods is for all investigated samples, and at almost all conversion rates below 1 kJ/kmol, therefore the lines are almost entirely overlapping. In the case of the Starink and OFW method, the differences are between 2-3 kJ/kmol, therefore the OFW curve is seen only for higher conversion rates or as a shadow for α<0.8. The activation energy of the initial and final stage seems to be a little underestimated by KAS, OFW, and Starink method, but the trends and values are in good agreement.

Values obtained from the decomposition of the sawdust are significantly higher compared to results reported in previous investigations. For the Friedman method, the mean activation energy is 241 kJ/mol, while for the other methods is slightly lower and about 229 kJ/mol. A similar underestimation of mean activation energy is also observed for the PUR sample. Zhang et al. [14] reported E_a for wood sawdust ~190 kJ/mol, Mishra and Mohanty [28] reported ~170 kJ/mol for pine wood, and 148-181 kJ/mol for sawdust depending on the used method. Alam et al. [16] reported even higher values (265-353 kJ/mol) for the bamboo sawdust for the conversion range (α=0.1-0.8). The activation energy of wheat straw is between 154-379 kJ/kmol, while beech sawdust individually has an activation energy in the range between 155-316 kJ/kmol [13]. Besides, Luo et al. [13] emphasized the importance of observing activation energy in the separate conversion ranges. Therefore, the division was made for the conversion ranges in the following way: first stage α=0.05-0.45, second stage α=0.45-0.7, and final stage α=0.7-0.85, after which the obtained values show strong divergence. A similar division can be applied for the sample used here as well. In the beginning, up to α=0.1, activation energy sharply increases due to moisture evaporation. After this point, the curve takes a gradual increase until the α=0.5. Most of the cellulose and hemicellulose content is decomposed in this stage, known as the active pyrolysis area. In the range α=0.5-0.8, the values remain constant, and lignin is mostly decomposed. In the final stage, the E_a sharply increases since most of the material is already decomposed. Once again, similar to the PUR sample, KAS, OFW, and Starink method seems to underestimate E_a values for the first stage of conversion since slightly visible differences are spotted. These differences are becoming less visible as the α continues to increase, and after α=0.6 are almost negligible.

The obtained values of the E_a with respect to the conversion rate (α) for investigated mixtures are more similar to SD than the PUR sample being in the range between 200-250 kJ/mol for most of the process. The mean E_a obtained for investigated mixtures is summarised in Table 3. As can be seen, the mixture with a small PUR content expresses the lowest values of E_a (~239 kJ/mol). This is an interesting observation since the individual SD expresses the highest values; therefore, it would be expected the same for the mixture where SD is a dominant compound. Nevertheless, the highest values are noted for the mixture with equal content of both compounds (~277 kJ/mol), which decreases with the further increment of PUR share to ~247 kJ/mol for the mixture with 75% of PUR. The sawdust influence is visible

from the conversion range up to α=0.2, where E_a gradually increases, similar to the SD sample. For the mixture where SD is a dominant compound, the second conversion stage is between α=0.2-0.7, where E_a continuously decrease. This is a completely reverse trend compared to the SD sample, which indicates the apparent influence of PUR content. After the conversion rate of α=0.7, values for E_a start to increase, suggesting that the conversion process has reached the final stage. In the mixture where polyurethane is a dominant compound, the second stage is between conversion rate α=0.2-0.6, once again with decreasing trend. Between α=0.6-0.7, a slight bounce of E_a is reported, followed by a steep increase until the end of the process. This slight bounce is also reported for individual PUR pyrolysis, even though it can be seen here that the values are shifted toward higher values of conversion rate. Mixtures with an equal share of each fraction express similar behaviour as the other two mixtures regarding the curve trend. Nevertheless, reported values of E_a are higher compared to other mixtures, especially after α=0.7. This implies that its heterogeneity limits the thermal degradation of mixtures, and therefore, the final mass and end of decomposition are achieved at lower conversion rates.

Comparison of E_a between investigated mixtures suggests that biomass plays a dominant role in the first part of the process (α<0.2), but in the second stage, PUR seems to have a more critical role. Even though the reported values of activation energy are more similar to SD, the decreasing trend noticed for all mixtures suggests that PUR has an important role in process dynamics. The last stage seems to be influenced the most by the mixture composition. In the case of the sample with 25% of PUR, the increase in the last stage is gradual and starts after the conversion rate of 0.7, while for the other two mixtures increase is steep and starts at α=0.6. Since the mixture where sawdust is the dominant compound also has the lowest final mass, this might suggest that the higher content of the PUR in the mixture hinders the thermal degradation of the sample. Nevertheless, since it is evident that the introduction of the PUR decreased the E_a in the main stage, it is more likely that the heterogeneity of the mixture is more influential for this part.

Table 3 - Activation energy and statistical agreement from investigated samples

Activation energy [kJ/mol]	Friedman		KAS		OFW		Starink	
	E_a	R^2	E_a	R^2	E_a	R^2	E_a	R^2
Sawdust	241.80	0.9629	229.33	0.9494	227.45	0.9591	229.54	0.9499
25% PUR	239.42	0.9793	235.95	0.9699	233.91	0.9743	236.17	0.9701
50% PUR	277.35	0.9485	272.85	0.9520	269.22	0.9572	273.05	0.9523
75% PUR	247.47	0.9785	240.80	0.9600	237.79	0.9664	241.02	0.9603
PUR	202.27	0.9985	192.00	0.9970	192.57	0.9973	192.28	0.9970

3.4 Analysis of thermodynamic parameters

In this section, apparent Friedman's activation energies are used to calculate the thermodynamic parameters such as pre-exponential factor and changes of free Gibbs energy, enthalpy, and entropy. In Figure 4, obtained E_a from Friedman method at 10 °C/min are plotted. This heating rate is used to reduce the impact of constituent interaction that increases

at higher heating rates. Once again, the PUR content's influence on the activation energies in the conversion range between 0.2 and 0.6 is evident, even though the obtained values are closer to SD values. Besides, it can be seen that at α=0.7, the activation energy of the mixtures has a steep increment, which is in line with the results from the TG analysis and the final mass of their residues.
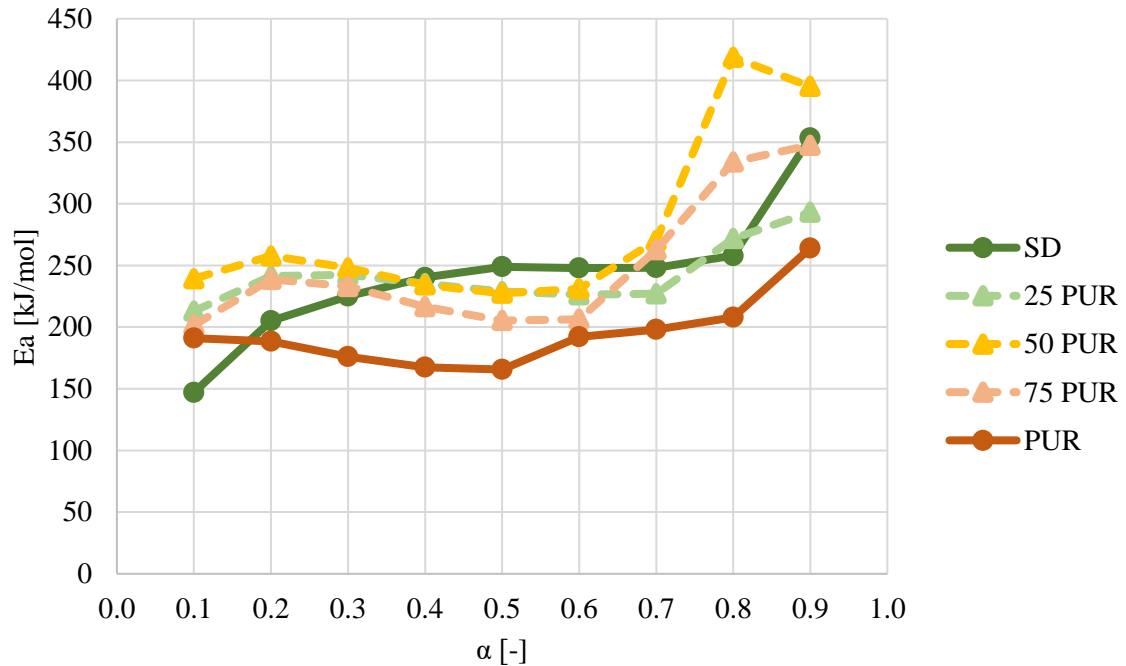
Figure 4 - Friedman's activation energies for investigated samples

The values of pre-exponential factors vary over the range of conversion Figure 5a. The pre-exponential factor was calculated based on Friedman's method and with the general assumption that a conversion function considers reaction order equals 1 [9]. In general, for all investigated samples, they are above 10^9 s^{-1} immediately after α=0.1. For the sawdust sample, these values are remarkably high ($10^{13}<A<10^{27}$) in the conversion range of $0.1<\alpha<0.9$. In the case of the PUR sample, these values are pronouncedly lower and, in the range, $10^{13}<A<10^{20}$. A decrease in the activation energy is followed up by a reduction of a pre-exponential factor in this range, which is then again followed up by the huge jump at higher conversion rates. Pre-exponential factors of investigated mixtures vary in a similar range as these from individual sample analysis. The steep increment is noticed after α=0.7, which is in line with the previously reported results. For all mixtures, the pre-exponential factors are closer to the SD sample. Based on the adopted assumption, the obtained pre-exponential factor represents the theoretical approach, and further research will consider the determination of specific conversion functions for all analysed samples, which will enable a more detailed analysis of pre-exponential factors. The Gibbs free energy (ΔG) changes are almost negligible for the conversion range $0.1<\alpha<0.9$, and only a slight decrease is noticed in all samples for approximately Δ5 kJ/mol. The highest values are calculated for the sawdust sample, which reduces with the increment of PUR content, and finally, the lowest values are reported for individual polyurethane decomposition (Figure 5b).

The enthalpy change (ΔH) indicates the difference in energy between the reagent and activated complex (Figure 5c). For the SD sample, ΔH increases with the conversion range, suggesting that lignin in biomass structure requires more energy for decomposition than hemicellulose and cellulose, which are decomposed in earlier stages. Nevertheless, reported values are high during the whole process, similar to lignin (~239 kJ/mol), indicating high lignin content or complex structure due to heterogenous sawdust composition. In comparison, the enthalpy change for maple leaf residue is only between 68-85 kJ/kmol [33]. On the other hand, the calculated values for the PUR are significantly lower (186-257 kJ/mol) and are following the trend of E_a and A. This means that the values firstly decrease until $\alpha=0.5$, and then increase until the end of the process, implying that the PUR sample has clear two stages of degradation, already described above. Firstly, the urethane bond and isocyanates are decomposed, followed by the decomposition of volatiles in the second stage between $\alpha=0.5$-0.8. The same trend is noticed for the investigated mixtures, even though obtained values are pronouncedly higher and closer to the SD sample. Since the values of ΔH in range $\alpha=0.3$-0.7 are lower for investigated mixtures than that of individual sawdust, it can be stated that the synergistic effect in that range has a beneficial impact of reducing required heat needed to form activated complex [34].

Entropy represents the disorder degree of the system. Lower entropy values imply that the system underwent some changes and has reached a new state of its own thermodynamic equilibrium. For the SD sample, entropy varies between -62.40 and 273.45 J/mol. This implies that the SD sample achieves a more ordered state at the beginning of the process since the moisture is evaporated and only solid-state remains. As the process proceeds, the solid sample starts to decompose, producing a high amount of gases, and therefore a change of entropy significantly increases with the increment of conversion rate. The evolution of gases from this sawdust mixture is confirmed in the investigation carried out by Stančin et al. [35]. For PUR, entropy starts to increase until $\alpha=0.12$ (20.53 J/mol) and then starts to decrease immediately to -28.51 J/mol for $\alpha=0.48$. After this point, an increment is observed once again until the end of conversion. The entropy of the mixture behaves in the same way as the PUR sample regarding the increasing-decreasing trend. Nevertheless, for the mixture, negative values are not reported at any stage of the process. The visible difference between the mixtures is the turning point at which conversion rate takes an increasing or decreasing trend. For the mixture where SD is the major compound, this is at $\alpha=0.14$ and $\alpha=0.66$, while for the PUR dominant mixture, this is at $\alpha=0.22$ and $\alpha=0.56$. In the case of a mixture with an equal share of both compounds, this is at $\alpha=0.16$ and $\alpha=0.54$. Results are given in Figure 5d.
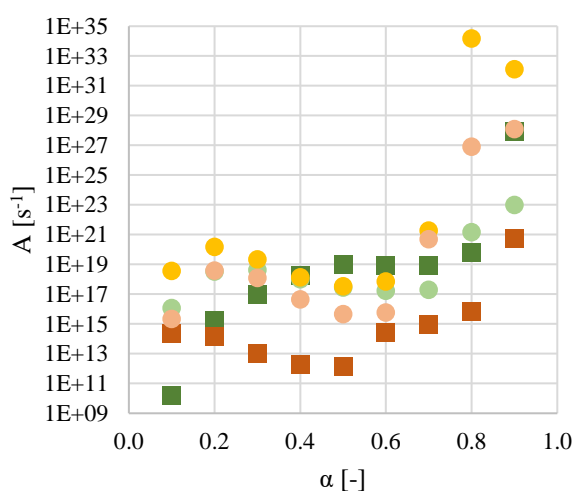
a)
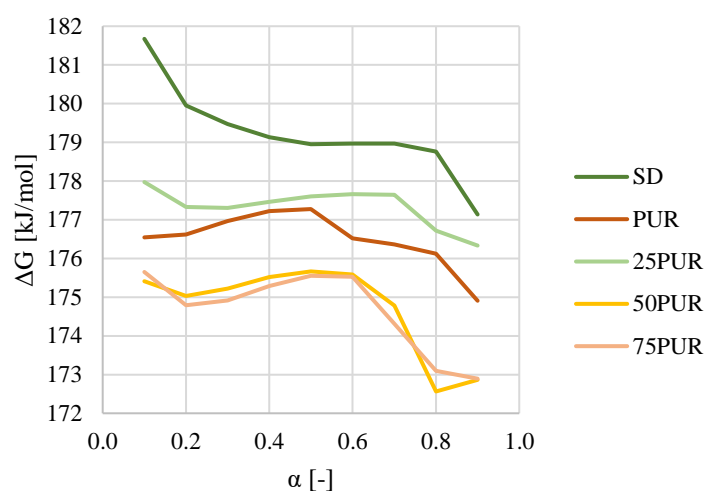
b)
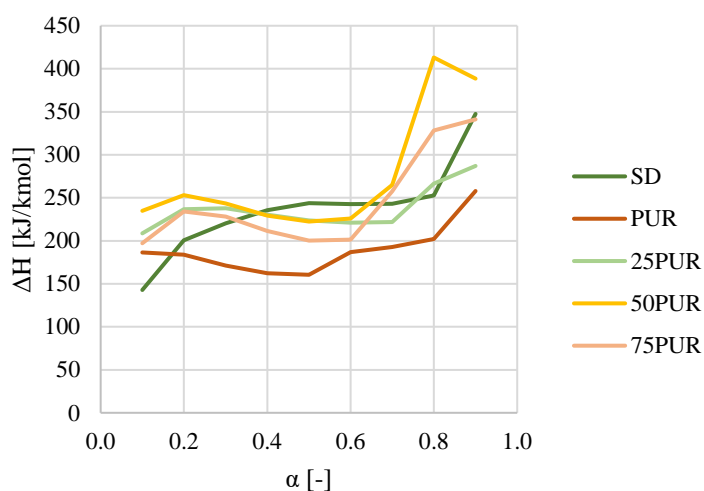
c)
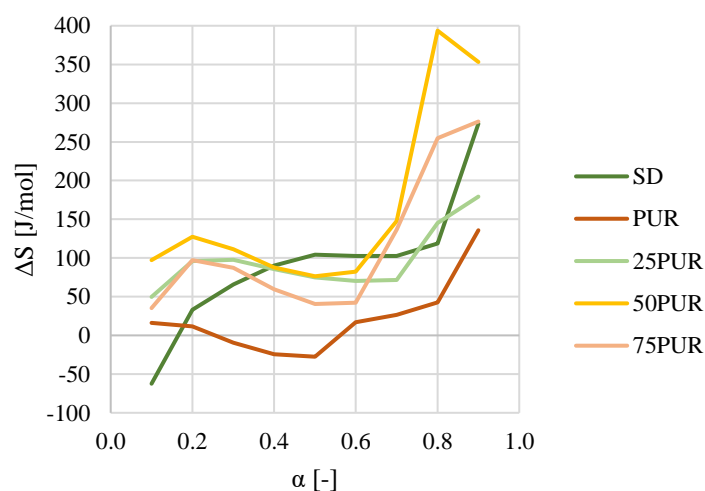
d)

Figure 5 - Thermodynamic parameters calculated at a heating rate of 10 °C/min

4. Conclusion

Thermogravimetric analysis of sawdust and polyurethane samples used in this study shows that their decomposition mechanism regarding the shape of the TG curve broadly correlates. This is due to the nature of PUR building units, which are more similar to biomass samples than conventional plastics. The main decomposition stages overlap in a temperature range between 300 and 400 °C, even though the chemical nature and reaction mechanism are entirely different. Thermogravimetric curves of the investigated mixtures are showing different behaviour, depending on the dominant constituent. Nevertheless, for the mixture with an equal share of SD and PUR, reported values of mass loss and thermal decomposition stages are closer to individual PUR analyses. The influence of the heating rate on thermal decomposition is evident since the increment in heating rate shifted peak temperatures and broaden the range in which degradation takes place for all investigated samples. For the individual PUR analysis and mixtures with 50 and 75% of PUR, an increment of heating rate

promotes the degradation, and lower final masses are reported. At the same time, a reverse trend is observed for SD and SD-dominant mixtures.

Calculated activation energies show that there is only a slight difference between the used methods. The KAS, OFW, and Starink methods underestimate E_a in the initial and final stages, while the values are similar for the main conversion range. The highest values are reported for individual SD pyrolysis, while the lowest ones are noted for polyurethane degradation. Besides, a constant increment of E_a is recorded for SD, while for the PUR, values first increase, then decrease, and finally jump to high values at the end of the process. This suggests a clear distinction between the two stages in PUR decomposition, which is also observed for analysed mixtures, even though reported values are closer to SD.

From the presented results, it is obvious that both heating rate and mixture composition have an important influence on process dynamics. As the heating rate increase, thermal degradation is broadened and shifted to higher temperatures. For the mixture composition, it can be stated that at some critical share of plastic content in the range between 25-50%, PUR starts to dominate the decomposition mechanism since the investigated parameters are following the trend similar to that of individual PUR, even though the values are closer to SD sample. For future work, the focus should be shifted to the SD-PUR mixture analysis with a lower share of plastic content (25-50%) since, in this range, unpredicted behaviour is observed. Even more, a critical point after which the plastic material starts to dictate the degradation mechanism might be located in this area.

References

[1]   PlasticsEurope; EPRO. Plastics – the Facts. Plast – Facts 2018 2018:38.

[2]   Simón D, Borreguero AM, de Lucas A, Rodríguez JF. Recycling of polyurethanes from laboratory to industry, a journey towards the sustainability. Waste Manag 2018;76:147–71. https://doi.org/10.1016/j.wasman.2018.03.041.

[3]   Crescentini TM, May JC, McLean JA, Hercules DM. Mass spectrometry of polyurethanes. Polymer (Guildf) 2019;181:121624. https://doi.org/10.1016/j.polymer.2019.121624.

[4]   Yao Z, Yu S, Su W, Wu D, Liu J, Wu W, et al. Probing the combustion and pyrolysis behaviors of polyurethane foam from waste refrigerators. J Therm Anal Calorim 2020;141:1137–48. https://doi.org/10.1007/s10973-019-09086-8.

[5]   Stančin H, Růžičková J, Mikulčić H, Raclavská H, Kucbel M, Wang X, et al. Experimental analysis of waste polyurethane from household appliances and its utilization possibilities. J Environ Manage 2019;243:105–15. https://doi.org/10.1016/j.jenvman.2019.04.112.

[6]   Guo X, Song Z, Zhang W. Production of hydrogen-rich gas from waste rigid polyurethane foam via catalytic steam gasification. Waste Manag Res 2020. https://doi.org/10.1177/0734242X19899710.

[7]   Jurić F, Stipić M, Samec N, Hriberšek M, Honus S, Vujanović M. Numerical investigation of multiphase reactive processes using flamelet generated manifold approach and extended coherent flame combustion model. Energy Convers Manag 2021;240:114261. https://doi.org/10.1016/j.enconman.2021.114261.

[8]   Garrido MA, Font R. Pyrolysis and combustion study of flexible polyurethane foam. J Anal Appl Pyrolysis 2015;113:202–15. https://doi.org/10.1016/j.jaap.2014.12.017.

[9]   Yao Z, Yu S, Su W, Wu W, Tang J, Qi W. Comparative study on the pyrolysis

kinetics of polyurethane foam from waste refrigerators. Waste Manag Res 2020;38:271–8. https://doi.org/10.1177/0734242X19877682.

[10] Mikulčić H, Jin Q, Stančin H, Wang X, Li S, Tan H, et al. Thermogravimetric analysis investigation of polyurethane plastic thermal properties under different atmospheric conditions. J Sustain Dev Energy, Water Environ Syst 2019;7:355–67. https://doi.org/10.13044/j.sdewes.d6.0254.

[11] Stančin H, Mikulčić H, Wang X, Duić N. A review on alternative fuels in future energy system. Renew Sustain Energy Rev 2020;128. https://doi.org/10.1016/j.rser.2020.109927.

[12] Ferreiro AI, Rabaçal M, Costa M. A combined genetic algorithm and least squares fitting procedure for the estimation of the kinetic parameters of the pyrolysis of agricultural residues. Energy Convers Manag 2016;125:290–300. https://doi.org/10.1016/j.enconman.2016.04.104.

[13] Luo L, Guo X, Zhang Z, Chai M, Rahman MM, Zhang X, et al. Insight into Pyrolysis Kinetics of Lignocellulosic Biomass: Isoconversional Kinetic Analysis by the Modified Friedman Method. Energy and Fuels 2020;34:4874–81. https://doi.org/10.1021/acs.energyfuels.0c00275.

[14] Zhang X, Deng H, Hou X, Qiu R, Chen Z. Pyrolytic behavior and kinetic of wood sawdust at isothermal and non-isothermal conditions. Renew Energy 2019;142:284–94. https://doi.org/10.1016/j.renene.2019.04.115.

[15] Manić NG, Janković BB, Dodevski VM, Stojiljković DD, Jovanović V V. Multicomponent Modelling Kinetics and Simultaneous Thermal Analysis of Apricot Kernel Shell Pyrolysis. J Sustain Dev Energy, Water Environ Syst 2020;N/A:0–0. https://doi.org/10.13044/j.sdewes.d7.0307.

[16] Alam M, Bhavanam A, Jana A, Viroja J kumar S, Peela NR. Co-pyrolysis of bamboo sawdust and plastic: Synergistic effects and kinetics. Renew Energy 2020;149:1133–45. https://doi.org/10.1016/j.renene.2019.10.103.

[17] Kim YM, Jae J, Kim BS, Hong Y, Jung SC, Park YK. Catalytic co-pyrolysis of torrefied yellow poplar and high-density polyethylene using microporous HZSM-5 and mesoporous Al-MCM-41 catalysts. Energy Convers Manag 2017;149:966–73. https://doi.org/10.1016/j.enconman.2017.04.033.

[18] Abbas-Abadi MS, Van Geem KM, Fathi M, Bazgir H, Ghadiri M. The pyrolysis of oak with polyethylene, polypropylene and polystyrene using fixed bed and stirred reactors and TGA instrument. Energy 2021;232:121085. https://doi.org/10.1016/j.energy.2021.121085.

[19] Samal B, Vanapalli KR, Dubey BK, Bhattacharya J, Chandra S, Medha I. Influence of process parameters on thermal characteristics of char from co-pyrolysis of eucalyptus biomass and polystyrene: Its prospects as a solid fuel. Energy 2021;232:121050. https://doi.org/10.1016/j.energy.2021.121050.

[20] Navarro M V., López JM, Veses A, Callén MS, García T. Kinetic study for the co-pyrolysis of lignocellulosic biomass and plastics using the distributed activation energy model. Energy 2018;165:731–42. https://doi.org/10.1016/j.energy.2018.09.133.

[21] ISO - ISO 14780:2017 - Solid biofuels — Sample preparation n.d.

[22] ISO 17225-1:2014(en), Solid biofuels — Fuel specifications and classes — Part 1: General requirements n.d.

[23] Yuan X, He T, Cao H, Yuan Q. Cattle manure pyrolysis process: Kinetic and thermodynamic analysis with isoconversional methods. Renew Energy

2017;107:489–96. https://doi.org/10.1016/j.renene.2017.02.026.

[24] Xu M, Guan J, Wang J. Pyrolysis behavior and kinetics of polyurethane insulation materials from waste refrigerators. Adv Mater Res 2012;356–360:1752–8. https://doi.org/10.4028/www.scientific.net/AMR.356-360.1752.

[25] Nishiyama Y, Kumagai S, Motokucho S, Kameda T, Saito Y, Watanabe A, et al. Temperature-dependent pyrolysis behavior of polyurethane elastomers with different hard- and soft-segment compositions. J Anal Appl Pyrolysis 2020;145:104754. https://doi.org/10.1016/j.jaap.2019.104754.

[26] Jiao L, Xu G, Wang Q, Xu Q, Sun J. Kinetics and volatile products of thermal degradation of building insulation materials. Thermochim Acta 2012;547:120–5. https://doi.org/10.1016/j.tca.2012.07.020.

[27] Jiao L, Xiao H, Wang Q, Sun J. Thermal degradation characteristics of rigid polyurethane foam and the volatile products analysis with TG-FTIR-MS. Polym Degrad Stab 2013;98:2687–96. https://doi.org/10.1016/j.polymdegradstab.2013.09.032.

[28] Mishra RK, Mohanty K. Pyrolysis kinetics and thermal behavior of waste sawdust biomass using thermogravimetric analysis. Bioresour Technol 2018;251:63–74. https://doi.org/10.1016/j.biortech.2017.12.029.

[29] Slopiecka K, Bartocci P, Fantozzi F. Thermogravimetric analysis and kinetic study of poplar wood pyrolysis. Appl Energy 2012;97:491–7. https://doi.org/10.1016/j.apenergy.2011.12.056.

[30] Oyedun AO, Tee CZ, Hanson S, Hui CW. Thermogravimetric analysis of the pyrolysis characteristics and kinetics of plastics and biomass blends. Fuel Process Technol 2014;128:471–81. https://doi.org/10.1016/j.fuproc.2014.08.010.

[31] Wang H, Wang QS, He JJ, Mao ZL, Sun JH. Study on the pyrolytic behaviors and kinetics of rigid polyurethane foams. Procedia Eng 2013;52:377–85. https://doi.org/10.1016/j.proeng.2013.02.156.

[32] Han B, Chen Y, Wu Y, Hua D, Chen Z, Feng W, et al. Co-pyrolysis behaviors and kinetics of plastics-biomass blends through thermogravimetric analysis. J Therm Anal Calorim 2014;115:227–35. https://doi.org/10.1007/s10973-013-3228-7.

[33] Ahmad MS, Klemeš JJ, Alhumade H, Elkamel A, Mahmood A, Shen B, et al. Thermo-kinetic study to elucidate the bioenergy potential of Maple Leaf Waste (MLW) by pyrolysis, TGA and kinetic modelling. Fuel 2021;293. https://doi.org/10.1016/j.fuel.2021.120349.

[34] Wen Y, Zaini IN, Wang S, Mu W, Jönsson PG, Yang W. Synergistic effect of the co-pyrolysis of cardboard and polyethylene: A kinetic and thermodynamic study. Energy 2021;229:120693. https://doi.org/10.1016/j.energy.2021.120693.

[35] Stančin H, Šafář M, Růžičková J, Mikulčić H, Raclavská H, Wang X, et al. Co-pyrolysis and synergistic effect analysis of biomass sawdust and polystyrene mixtures for production of high-quality bio-oils. Process Saf Environ Prot 2021;145:1–11. https://doi.org/10.1016/j.psep.2020.07.023.